Available online at www.sciencedirect.com
SCIENCE DIRECT®
Coordination Chemistry Reviews 248 (2004) 477–492
COORDINATION CHEMISTRY REVIEWS
www.elsevier.com/locate/ccr

Review

# Viologen embedded zeolites

Edward L. Clennan*

*Department of Chemistry, University of Wyoming, Laramie, WY 82071, USA*

Received 6 September 2003; accepted 6 November 2003

## Contents



## Abstract

Reactions between molecules leading to new materials are complex processes. In an effort to understand these complex systems chemists have understandably attempted to minimize complexity. This has resulted in a distinct preference for study of reactions in homogenous, rather than in heterogeneous media, despite the fact that heterogeneous reactions in real world situations are ubiquitous. Nevertheless, the advantages of heterogeneous systems in terms of environmental friendliness and in the ability to control reaction outcome are widely recognized and as a result are attracting increased attention. Zeolites are excellent examples. The early use of zeolites focused entirely on their use as acid catalysts in petroleum processing and only recently has attention turned to their use in fine chemical synthesis. In this review we present recent results in the design and use of the very interesting heterogeneous host–guest viologen/zeolite complexes.


*Keywords:* Zeolites; Mordenite; Periodic mesoporous organosilica

## 1. Introduction

The chemistry of viologens [1–3] and of zeolites [4–6] have been extensively reviewed. The marriage of these two

* Tel.: +1-307-766-6667; fax: +1-307-766-2807.
*E-mail address:* clennane@uwyo.edu (E.L. Clennan).

0010-8545/$ – see front matter © 2004 Elsevier B.V. All rights reserved.
doi:10.1016/j.ccr.2004.01.001

areas represents a more recent development [7] whose potential has not been completely exploited. In this review we begin with a brief introduction to both zeolites and viologens and then move on to an exploration of these new materials.

### 1.1. Zeolites

Zeolites are crystalline solids consisting of catenated silicon and aluminum tetrahedra that enclose regular repeating cavities or channels of well-defined size and shape [8]. These novel materials are generally synthesized by hydrothermal synthesis routes from gels at temperatures between 80 and 200 °C [9]. Over 30 naturally occurring zeolites have been identified and over 100 zeolites without a natural occurring counterpart have been synthesized [10]. In addition to these zeolites a large number of zeotypes containing other framework atoms, such as P, S, B, and V have also been synthesized. The structure committee of the International Zeolite Association (IZA; http://www.iza-online.org/) has assigned, with the authority granted by IUPAC, 139 different framework type codes (three capital letters) to these materials. These mnemonic codes do not depend on composition (i.e. distribution of the tetrahedral atoms) but only describe the three-dimensional labyrinth of framework atoms. A selection of different zeolites with their framework codes are illustrated in Fig. 1 [11a]. The vertices in these structures represent the tetrahedral atoms and the lines represent bridging oxygen atoms. These structures also are representative of five major groups (eight-membered ring, medium, dual, large, and meso) classified on the basis of their pore/channel systems [10]. NaY (FAU) is a large pore zeolite characterized by windows 7.4 Å in diameter tetrahedrally arranged about a 13 Å diameter supercage. Mordenite (MOR) is a dual pore system with interconnecting channels (7.0 Å × 6.7 Å and 2.6 Å × 5.7 Å). Mazzite (MAZ) is also a dual pore system (7.4 Å × 7.4 and 3.4 Å × 5.6 Å) with 12 and 8-oxygen ring interconnecting channels. Linde Type A (LTA) is a eight-membered ring pore system with octahedrally arranged 4.2 Å windows surrounding a 11.4 Å cage. ZSM-5 (MFI) is a medium pore zeolite consisting of two interconnecting channels (5.3 Å × 5.6 Å and 5.1 Å × 5.5 Å). VPI-5 (VFI) is a meso pore zeolite with a one-dimensional 18-oxygen ring channel pore system with 12 Å pore size. In addition to these microporous materials, (pore diameters ≤≈ 20 Å) a new class of mesoporous (pore diameters ≈ 20–500 Å) zeolites, such as MCM-41 [12], with hexagonal pore systems are also available.

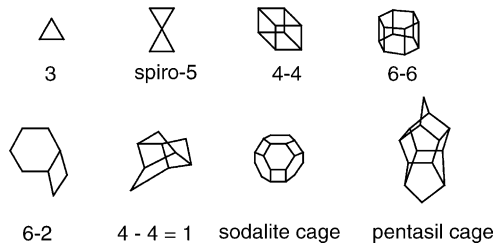


Fig. 2. SBUs and the sodalite and pentasil structural units.

Discussion of zeolites using the concept of secondary building units (SBUs) is a useful way of visualizing these interesting structures. These non-chiral repeating units consist of up to 16 tetrahedral atoms ($TO_4$) and are always found in an integral number within the unit cell. A selection from the 20 SBUs currently recognized by the IZA is depicted in Fig. 2 along with two other useful structural units; the sodalite and pentasil cages. The supercage in FAU (Fig. 1) is surrounded by 10 sodalite units connected via the 6-rings by bridging oxygens. On the other hand, the 11.4 Å cage in LTA (Fig. 1) is surrounded by eight sodalite units connected via the four-rings via bridging oxygens. The pentasil structural unit is also found in several zeolites including MOR (Fig. 1) and ZSM-5.

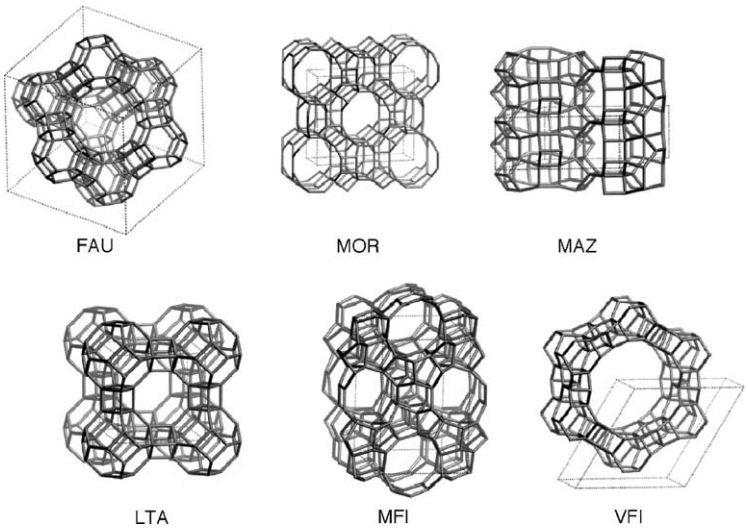


Fig. 1. IUPAC framework codes for a selection of zeolites [code (example)] including a large pore [FAU (NaY)], dual pore system [MOR (mordenite)] and [MAZ (Mazzite)], eight-membraned ring pore system [LTA9Linde Type A], medium pore [MFI (ZSM-5)], and meso pore sysrem [VFI (VPI-5)].

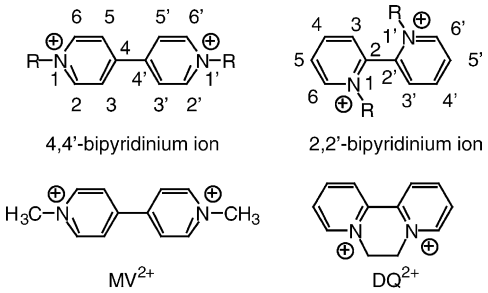


Fig. 3. Viologen numbering scheme.

Zeolites had a dramatic impact on petroleum processing in the 1960s. Recent developments have seen a dramatic expansion in their use for the synthesis of fine chemicals [13]. These novel materials have several attractive characteristics that have contributed to their increasing use as heterogeneous catalysts. These characteristics include: (1) the ability to fine tune the interior electrostatic environment by ion exchange of the cations associated with the tetrahedral aluminum atoms; (2) the ability to fine tune the acid properties by ion exchange and/or framework manipulation; (3) the ability to dry these materials in air at elevated temperatures (e.g. 300–500 °C) without structural damage; and (4) the ability of these materials to discriminate between substrates and/or products based upon size and shape selectivity (molecular sieving property).

### 1.2. Viologens

The name viologen has been used to describe the diquaternary salts of 4,4′- and 2,2′-bipyridines (Fig. 3). The 4,4′-viologen, also known as methyl viologen or paraquat ($MV^{2+}$; Fig. 3), was first reported in 1882 by Weidel and Russo [14]. Despite much early work with these interesting compounds the examination of their chemistry did not fully blossom until the mid 1950s when it was discovered that diquat ($DQ^{2+}$; Fig. 3) was a potent herbicide. The synthesis and properties of these interesting materials have been extensively and expertly reviewed [1–3,15] and as a consequence only a brief description of their attributes pertinent to their intrazeolite behavior is provided in this review.

#### 1.2.1. Redox behavior

Perhaps the best known attribute of the viologens is their ability to exist in three well-characterized oxidations states, the dication, the radical cation, and the neutral forms (Fig. 4). The availability of these oxidation levels play important roles in the use of viologens as redox indicators in biological systems, as electrochemical display devices, and even in their herbicidal activity.

The electrochemical behavior of viologens have been extensively examined [16]. In organic solvents both redox couples (dication → cation radical and cation radical → neutral) are reversible for most viologens. The second redox couple, however, is in general irreversible in water as a result of the insolubility of the neutral partner. The reversible dication cation radical reduction potentials for several viologens in $CH_3CN$ are reported in Table 1. The reduction potentials for the cation radical → neutral redox couples are sufficiently cathodic of these values to make the disproportionation reaction (Eq. (1)) unfavorable (e.g. a value of $K = 1.7 \times 10^{-7}$ has been reported for $MV^{2+}$ in acetonitrile) [17].

Table 1
Reduction potentials for viologen dication → cation radical redox couples[a]

| Viologen | $E_{1/2}$ (V) vs. SCE |
|---|---|
| 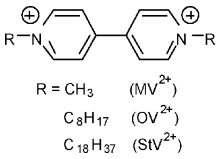 R = $CH_3$ ($MV^{2+}$); $C_8H_{17}$ ($OV^{2+}$); $C_{18}H_{37}$ ($StV^{2+}$) | −0.45[b] (−0.43)[c]; −0.42[c]; −0.46[c] |
| 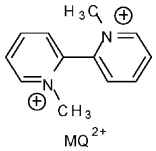 MQ 2+ | −0.76[b] (−0.75)[c] |
| 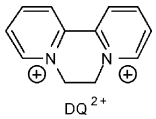 DQ 2+ | −0.39[d] (−0.36)[c] |
| 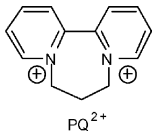 PQ 2+ | −0.56[b,c] |
| 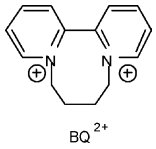 BQ 2+ | −0.67[b] (−0.66)[c] |
| 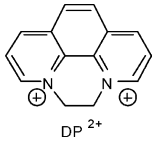 DP 2+ | −0.32[c] |

[a] In $CH_3CN$ vs. SCE.
[b] U. Ammon, C. Chiorboli, W. Dümler, G. Grampp, F. Scandola, H. Kisch, *J. Phys. Chem. A*, 101 (1997) 6876–6882.
[c] I. Nunn, B. Eisen, R. Benedix, H. Kisch, *Inor. Chem.* 33 (1994) 5079–5085.
[d] K.B. Yoon, J.K. Kochi, *J. Am. Chem. Soc.* 110 (1988) 6586–6588.

$$2\text{Viologen}^{\bullet+} \rightarrow \text{Violgen}^{2+} + \text{Viologen}^{\circ} \quad (1)$$

#### 1.2.2. Structure

The structures of 2,2′- and 4,4′-viologen dications have been extensively investigated by both theoretical and experimental methods [3]. The agreement between these two methods is excellent except in those cases in which the counterions interact with the viologen core by a charge transfer (CT) mechanism [3]. In those cases the charge

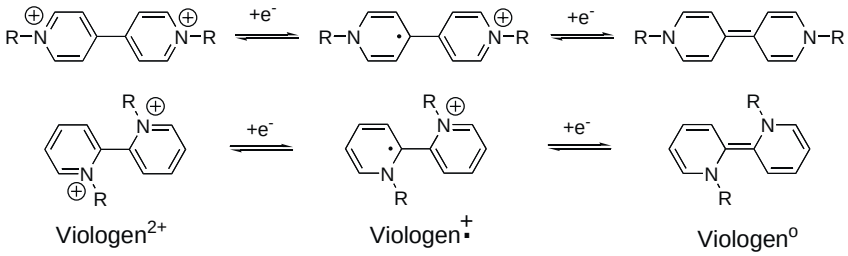


Fig. 4. Viologen redox states.

transfer induces a structural change in the viologen core that partially mimics the change that occurs upon complete reduction to the radical cation (vide infra).

The bipyridinium rings in conformationally unrestricted 2,2′- and 4,4′-viologen dications prefer to adopt a non-coplanar arrangement presumably as a compromise between steric and electronic factors. Experimental and theoretically determined structures for several viologen dications are depicted in Fig. 5. The bond lengths, bond angles, and the bipyridinum ring torsional angle in $DQ^{2+}$ are nearly identical in the X-ray [18] and molecular mechanics structure [19]. On the other hand, the 40° B3LYP/6-31G(d) torsional angle [11b] in $MV^{2+}$ is very different than the near 0° torsional angle observed in the halide ($Cl^-$, $Br^-$, and $I^-$) salts [20] but very similar to the 50° torsional angle observed in the non-interacting $PdCl_4^{2-}$ salt [21]. Willner and coworkers [19] have demonstrated that the reduction potentials of 2,2′- and presumably 4,4′-viologens are linearly related to the torsional angle between the two pyridinium rings. The torsional angle was suggested to be a "general measure" for the energetic barrier to force the viologen into a planar conformation where full $\pi$–$\pi$ resonance overlap in the radical cation can occur.

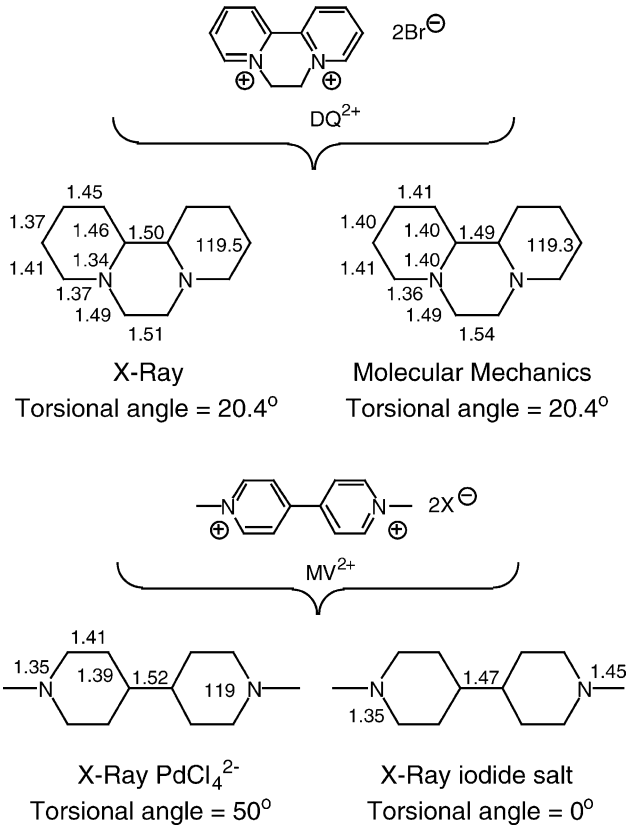


Fig. 5. Selected bond lengths and angles for $MV^{2+}$ and $DQ^{2+}$.

Methyl viologen radical cation, $MV^{+\bullet}$, is the only viologen radical cation whose crystal structure has been reported [22]. Nevertheless, many viologen radical cations can be made in solution and their structures spectroscopically characterized. Methyl viologen radical cation, $MV^{+\bullet}$, has been suggested to adopt a near planar geometry that maximizes delocalization. The UV-Vis spectra of methyl viologen radical cation, $MV^{+\bullet}$, exhibits an intense absorption at approximately 390 nm ($\varepsilon = 30{,}000\ M^{-1}\ cm^{-1}$) and at 605 nm ($\varepsilon = 10{,}700\ M^{-1}\ cm^{-1}$), which is responsible for its characteristic deep blue color [23], and is consistent with a planar geometry. IR spectra [24,25] and a normal coordinate analysis of $MV^{+\bullet}$ [26] reveals an increased bond order in comparison to $MV^{2+}$ for the bond interconnecting the two pyridinium rings providing additional support for a near planar structure. Several theoretical studies also confirm the greater propensity of $MV^{+\bullet}$ in comparison to $MV^{2+}$ to adopt a planar geometry [27,28].

Radical cations derived from 2,2′-bipyridinium ions have also been characterized. For example, $DQ^{+\bullet}$ is green [29] and exhibits an $\varepsilon$ of $3109\ M^{-1}\ cm^{-1}$ at 760 nm [30]. However, conformational unrestricted 2,2-bipyridinium cation radicals are not planar. $MQ^{+\bullet}$ (Fig. 6) at the B3LYP level of theory with a 6-31G(d) basis set exhibits minima at NCCN dihedral angles of approximately 45 and 135° [31]. As a result of this severely twisted geometry the radical cation does not enjoy delocalization and is significantly destabilized.

The neutral redox partners, viologen (Fig. 4) are by far the least well characterized of the three redox forms. $MV^{\circ}$ has been generated in acetonitrile and in tetrahydrofuran by magnesium and sodium reduction of $MV^{2+}$ [32]. It is characterized by a $\lambda_{MAX}$ of 396 nm ($\varepsilon = 27{,}000$) and the absence of the absorption band near 600 nm that acts as a fingerprint for $MV^{+\bullet}$. The NMR shifts ($C_6D_6$) of the ring protons at 5.52 and 5.31 ppm are significantly upfield of the aromatic-like values of 9.21 and 8.68 ppm observed for $MV^{2+}$, and the

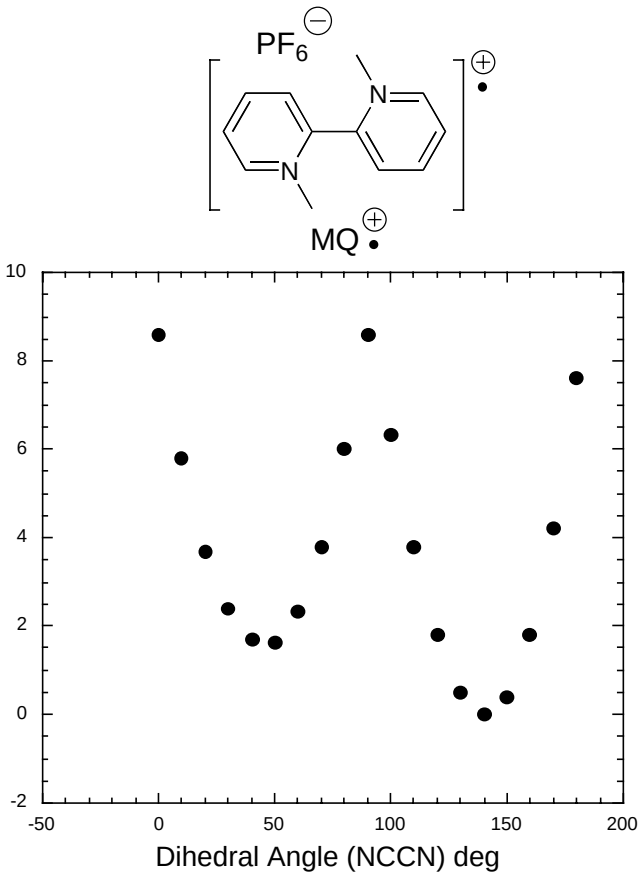


Fig. 6. Rotational profile of $MQ^{\oplus\bullet}$ at the B3LYP/6-31 (d) level.

N-$CH_3$ chemical shift of 2.10 ppm is that expected for a simple amine rather than a methyl on a positively charged nitrogen (4.56 ppm in $MV^{2+}$). These data are all consistent with the closed shell enamine-like structure given in Fig. 4.

*1.2.3. Charge transfer complexes*

Another well established attribute of viologens is their propensity to function as the electron poor partner in CT complexes. These electron-donor/electron acceptor interactions have been extensively examined in solution [33] and have played a key role in the development of modern theories of electron transfer [34]. Viologen intra- and intermolecular CT complexes have been documented with a wide range of donors including halides [35,36], ferrocyanide [37], carboxylate anions [38], amines [39], phenols, and arenes [40]. These CT complexes are characterized by very small association constants ($K_{CT} \approx 0.2$–$2\,M^{-1}$) indicative of a weak interaction. Nevertheless, isolation of bright orange crystals of the $MV^{2+}$/2,6-dimethoxynapthalene CT complex has been reported [41]. Interestingly, the face-to-face alignment (interannular separation 3.46 Å) [42] shows a crossed orientation of the long axes of the CT partners with the association localized over only one of the pyridinium rings [43].

## 2. Construction of viologen/zeolite host–guest complexes

Viologens have been introduced into zeolites by three different protocols: (1) ion exchange; (2) ship-in-a-bottle synthesis, and (3) periodic mesoporous organosilica (PMO) synthesis.

In 1989, Yoon and Kochi reported the ion exchange introduction of both $MV^{2+}$ and $DQ^{2+}$ (Fig. 3) by addition of NaY (Fig. 1) to an aqueous solution of $MVCl_2$ and $DQBr_2$ [41]. $MV^{2+}$, in particular, has subsequently been introduced by ion exchange into a wide variety of zeolites including sodium mordenite (MOR) [43], zeolite L [43], mazzite (MAZ or Ω), [43] sodium β [44], NaZSM-5 [44], NaX [44], and HMCM-41 [44]. This ion exchange procedure is very convenient since the intercalation of the viologen into the zeolite can be monitored by several techniques including UV-Vis examination of the supernatant aqueous solution.

The dimensions of the zeolite pore system, the viologen volume/dimensions, and the number of exchangeable cations provide limits on the amount of viologen that can be successfully incorporated. For example, it has been demonstrated that a maximum of two molecules of $MV^{2+}$ and $DQ^{2+}$ can be incorporated into the supercage of NaY [43]. This is reasonable given the 7.4 Å entrance window and the 13 Å diameter and 827 $Å^3$ supercage volume [45] of NaY and the molecular dimensions of $MV^{2+}$ and $DQ^{2+}$ ($MV^{2+}$ has a molecular volume of approximately 255 $Å^3$ and can be viewed as a cylinder 5 Å in diameter with a length of 11 Å; $DQ^{2+}$ has a molecular volume of approximately 285 $Å^3$ and can be viewed as a cylinder 6 Å in diameter and 11 Å in length) [46]. This result is also consistent with the number of sodium cations reasonably available (5 per supercage) for exchange in NaY. These cations occupy three different sites (Fig. 7) and have been referred to as Type I (16 per unit cell or 2 per supercage), Type II (32 per unit cell or 4 per supercage), and Type III (8 per unit cell or 1 per supercage). On the other hand, neither $MV^{2+}$ nor $DQ^{2+}$ intercalates into zeolite A with a 4.2 Å pore size consistent with the estimates of their molecular sizes [43].

Intercalation of the viologen (ion exchange) with one of its associated counterions (e.g. $MVCl^+$), although possible, is

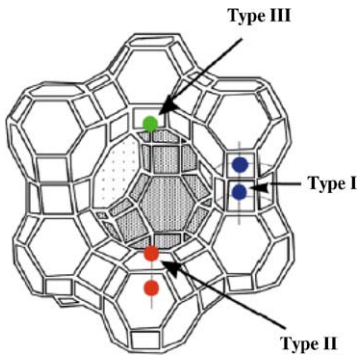


Fig. 7. Location of exchangeable (Type II and Type III) and non-exchangeable (Type I) cations in NaY.

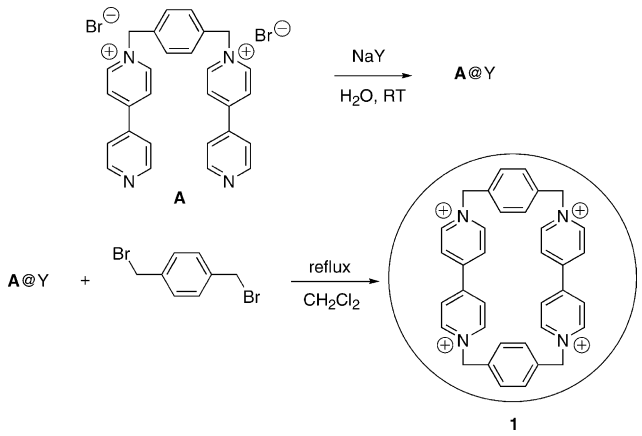


Fig. 8. Ship-in-a-bottle synthesis of a viologen.

highly unlikely. Alvaro and coworkers [44] have used X-ray photoelectron spectroscopy to demonstrate the lack of chloride incorporation during ion exchange with NaZSM-5 and MCM-41. Counterion ($Cl^-$) incorporation would be more likely in these zeolites than in the other zeolites examined because of their high Si/Al ratio, lower cation content, and the anticipated greater distance separating the negative centers on the framework.

The "ship-in-a-bottle" synthesis of viologen imbedded zeolites has rarely been employed. Nevertheless, the "ship-in-a-bottle" synthesis of bis-viologen, **1**, (Fig. 8) has recently been reported [47]. This particular viologen is ideally suited for this incorporation method since its dimension ($7.4 \times 10^3$ Å) is too large to allow intercalation from solution but it is the correct size to fit within the 13 Å supercage of NaY [48]. In addition, a high yield ship-in-a-bottle bis-alkylation step generating byproducts conveniently removed by solid–liquid extraction is available (Fig. 8). The preferred intrazeolite U-shape geometry of precursor A (Fig. 8) that mimics the geometry of this fragment in the product also promotes product formation. This templating effect along with the highly selective bis-alkylation step guarantees a high yield ship-in-a-bottle synthesis.

PMO synthesis [49], like "ship-in-a-bottle synthesis, has rarely been employed to generate viologen embedded zeolites but it has great potential to produce novel new inorganic–organic hybrid materials with useful properties. This protocol involves typical hydrothermal crystallization techniques [9] using appropriately silylated organic precursors and structural-directing agents. The presence of the silylated organic precursor generates a material in which the organic fragment is directly embedded in the zeolite framework. The first application of this technique to generate a viologen PMO of the MCM-41 type is illustrated in Fig. 9 [50]. This reaction uses tetraethylorthosilicate (TEOS) as the silicon source, cetyltrimethylammonium bromide (CTABr) as the structural directing agent, and *N*,*N*′-bis(trimethylsilylpropyl)-4,4′-bipyridinium diiodide, **2**, as the viologen source (Fig. 9). A recent investigation of this new material suggests that it has distinctly different properties than the corresponding ion-exchanged materials [51]. A vinylogous viologen PMO synthesized by incorporation of *trans*-1,2-bis[*N*-(trimethyloxysilylpropyl)pyridiumyl] ethylene (**A** in Fig. 9) has also recently been reported [52]. Irradiation of this material appears to induce a *cis–trans* isomerization and a marked change in the surface area and pore volume.

## 3. Structural characterization/spectroscopic properties of viologen/zeolite host–guest complexes

Dealkylation/decomposition of viologens can occur during incorporation into the zeolite using any of the synthetic protocols outlined in the previous section. Fortunately, the structural integrity of the viologen in these viologen-embedded zeolites can be verified with a remarkably wide range of spectroscopic and non-spectroscopic structural tools. These tools include fluorescence spectroscopy, Raman spectroscopy, infrared spectroscopy (IR), $^{13}C$ NMR, thermogravimetry, diffuse reflectance UV-Vis spectroscopy, and X-ray photoelectron spectroscopy (XPS).

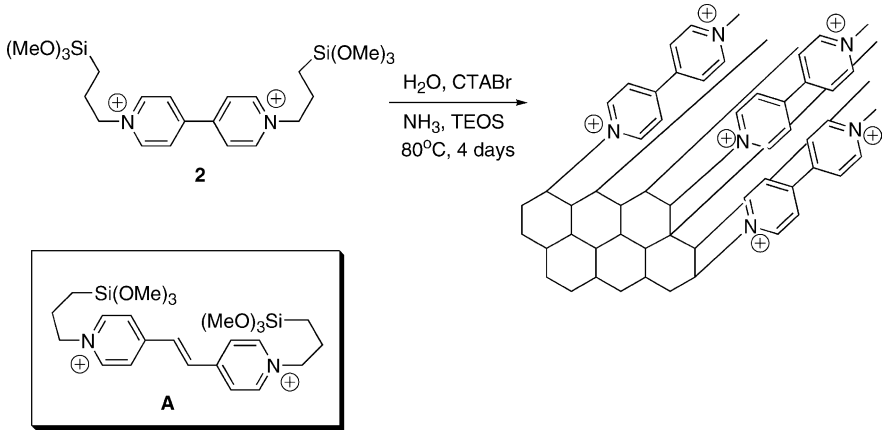


Fig. 9. PMO synthesis.

In addition to providing structural information many of these tools also provide valuable insight into specific interactions between the viologen and the zeolite host.

### 3.1. UV-Vis spectroscopy

Zeolites do not contain chromophores that absorb electromagnetic energy in the UV-Vis region of the spectrum. Consequently, optical probing of embedded guests is possible using diffuse reflectance techniques [53]. These techniques measure the difference in the scatter light absorbed by a pure white surface reference and that absorbed by the embedded guest. In general, integrating spheres are used to collect the low intensity of scattered light generated by this method. The reflected light ($R'_\infty$) is plotted according to the Kubelka–Munk equation (Eq. (2)) to give an optical spectrum similar to the transmission spectrum obtained in normal UV-Vis absorption spectroscopy. The absorption coefficient, $K$, under conditions of low guest concentration and high standard surface area is proportional to the concentration of the embedded guest reminiscent of the Lambert–Beer Law.

$$F(R'_\infty) = \frac{(1 - R'_\infty)^2}{2R'_\infty} = \frac{K}{S} \quad (2)$$

$K$ is the absorption coefficient; $S$ the scattering coefficient.

The absorption maximum for $MV^{2+}$ is a sensitive function of counterion and solvent [54,55]. With non-interacting counterions $MV^{2+}$ is colorless but with the strongly interacting iodide a charge transfer interaction occurs to give a brilliant scarlet colored solid [3]. Park and coworkers [56] reported a $\lambda_{MAX}$ of 265 nm for $MV^2$ in NaY; slightly different than that observed in solution in the presence of non-interacting counterions ($\lambda_{MAX} = 257$ nm; $\varepsilon = 20{,}800$ in $H_2O$) [55]. A careful examination of the diffuse reflectance spectra of a series of $MV^{2+}$ doped alkali metal-exchanged Y zeolites also revealed a red-shift with increasing size of the alkali metal ($Li^+$ 264 nm; $Na^+$ 265 nm; $K^+$ 268 nm; $Rb^+$ 271 nm; $Cs^+$ 272 nm). Inspection of the diffuse reflectance spectra revealed that the red-shift of the higher energy fronts of the absorption bands were responsible for the change in $\lambda_{MAX}$. Deconvolution of the absorption bands resulted in identification of contributions of a broad high-energy band and a narrow low-energy band to the overall absorption profile. The observation that the high-energy band was broad and that its $\lambda_{MAX}$ correlated with the donor strength of the zeolite framework is consistent with a charge transfer interaction between $MV^{2+}$ and zeolite framework.

### 3.2. Fluorescence spectroscopy

The lack of zeolite chromophores in the UV and visible region also means that light emitted by viologens will not be absorbed and can be detected with conventional fluorimeters equipped with front-face attachments that prevent reflected excitation light from reaching the detector [57].

The fluorescence of $MV^{2+}$ in solution and in zeolites has been the source of considerable controversy. Many authors claim that aqueous solutions of methyl viologen, $MV^{2+}$, are non-fluorescent [55] while others report weak but easily discernible emission intensity at 345 nm [58,59]. The intensity of a reported [54] green fluorescence (≈520 nm) appears to be dependent on the history/source of the sample of $MV^{2+}$ and upon the absence or presence of oxygen. These observations induced Mau et al. [55] to speculate that the 520 nm fluorescence is due to adventitious formation of 1′,2′-dihydro-1,1′-dimethyl-2′-oxo-4,4′-bipyridinium cation, **3**, although other green emitting species were also observed but were not identified. In contrast to $MV^{2+}$, viologen **4**, 1,1′,2,2′,6,6′-hexamethyl-4,4′-dipyridinium dication fluoresces in aqueous media at 360 nm from its $S_1$ ($\pi^* \leftrightarrow \pi$) state with a quantum yield of 0.081 [55], and $DQ^{2+}$ (Fig. 3) fluoresces with a quantum yield of 0.03 [60]. The congruence of the aqueous absorption and photoexcitation spectra of **4** rules out the possibility of emitting impurities. It is not entirely clear why $MV^{2+}$ and **4** exhibit different emission properties in water. However, the six methyl groups in **4** might sterically protect its $S_1$ state from quenching by the counterion and/or solvent.Significant emission of $MV^{2+}$ in

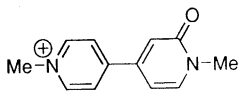

**3**

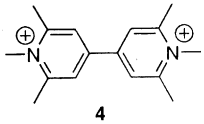

**4**

acetonitrile has recently been attributed to the high ionization potential (IP) and the lack of electron transfer quenching of $MV^{2+*}$ by this difficult to oxidize solvent [59].

Villemure et al. [58] have reported that $MV^{2+}$ in the interlamellar region of several smectite clays, including montmorillonite, emits easily detectable fluorescence. The interlamellar space of only 0.30 nm in montmorillonite forces $MV^{2+}$ to adopt a planar geometry and severely restricts rotation around the interpyridinium ring bond. The authors speculate that since rotation around this bond provides the main pathway for non-radiative deactivation of the excited singlet state that the structural confinement itself is responsible for the observation of fluorescence. These authors also demonstrated that the fluorescence is quenched by iron and exhibits a distribution of lifetimes consistent with heterogeneity of the clay structure and population of different absorption sites [61].

$MV^{2+}$ embedded in NaZSM-5, NaY, Na-mordenite, and CsY emits fluorescence at 330 and 420 nm [57]. The counterions in these zeolites are presumably the negative framework aluminum atoms. Consequently, the observed emission in these materials might be due to the curvature of the zeolite wall that prevents close approach to the counterions preventing the quenching observed in solution. In addition, photoexcitation spectra in NaY demonstrate that

different species are responsible for the 330 and 420 nm emissions. The authors have suggested based upon molecular modeling and $^{13}C$ CP/MAS NMR results that the 330 nm emission is from a planar conformation of $MV^{2+}$ and the 420 nm emission from a twisted conformer associated with the basic oxygen atoms in the zeolite framework [57]. This interpretation, however, is not universally accepted [59] and more work is clearly needed to understand the photophysical behavior of viologens in zeolites and in solutions.

### 3.3. FT-IR/Raman spectroscopy

The functional group region from 3400 to 1200 $cm^{-1}$ is relatively free of zeolite framework vibrations making both FT-IR and Raman spectroscopy extremely valuable tools to characterize viologen embedded zeolites. Use of diffuse reflectance accessories or nujol/fluorolube mulls (Fig. 10) are all appropriate for FT-IR data collection. The IR spectra of NaMVY and NaMQY shown in Fig. 10a and b are dominated by the water stretching band at 3500 $cm^{-1}$ and bending band at 1630 $cm^{-1}$ and directly reflect the hydrophilic character of most zeolites. These bands can be minimized by taking the IR spectra in sealed cells of samples dehydrated at elevated temperatures and reduced pressures.

The IR [24,25] and Raman spectra [62,63] of $MV^{2+}$ have both been exhaustively examined and complete assignments of specific vibrational bands have been made. Calzaferri and coworkers [64] have examined $MV^{2+}$ in zeolite L and demonstrated the analytical potential of in situ FT-IR and Raman spectroscopy as well as the ability of these techniques to detect interactions between the host and guest. For example, these workers used the appearance of the $\nu(N^{+}\text{-}CH_3)$ peak in the $MV^{2+}$ embedded zeolite-L Raman spectrum to argue that the viologen is twisted about the bond connecting the two pyridyl rings. In addition, they also used the framework vibration bands as internal standards for determination of loading levels.

### 3.4. Solid state NMR

Solid state NMR is perhaps the least useful of the spectroscopic techniques that can be applied to the examination of viologen embedded zeolites. MAS $^{13}C$ NMR spectra are often characterized by poor resolution, which is due in part to the interaction of the viologen with the quadrupolar aluminum and as a result of heterogeneous population of the viologen in various zeolite framework locations. Nevertheless, several authors have reported MAS $^{13}C$ NMR spectra of viologen embedded zeolites, which have assisted in their characterization [42,44,47]. $^{13}C$ labeling dramatically improves the signal to noise and can provide insight into these heterogeneous samples [65]. NMR techniques are not suitable at all for the study of the paramagnetic embedded viologen radical cations.

### 3.5. Electrochemistry

The anticipation that zeolites could potentially influence electrochemical reactions by both physical and chemical means has produced a large number of studies with zeolite modified electrodes [66]. Recent electrochemical work with $MV^{2+}$ doped Y zeolite has focused on distinguishing between intra- and extrazeolite mechanisms for reduction of $MV^{2+}$ [67–70]. Enhanced current at the potential of the second reduction has been attributed to a conproportionation reaction ($MV^{2+} + MV^{\circ} \rightarrow 2MV^{+}_{\bullet}$) which reforms the electroactive radical cation [71]. Recent results which demonstrates that a size and charge excluded surfactant

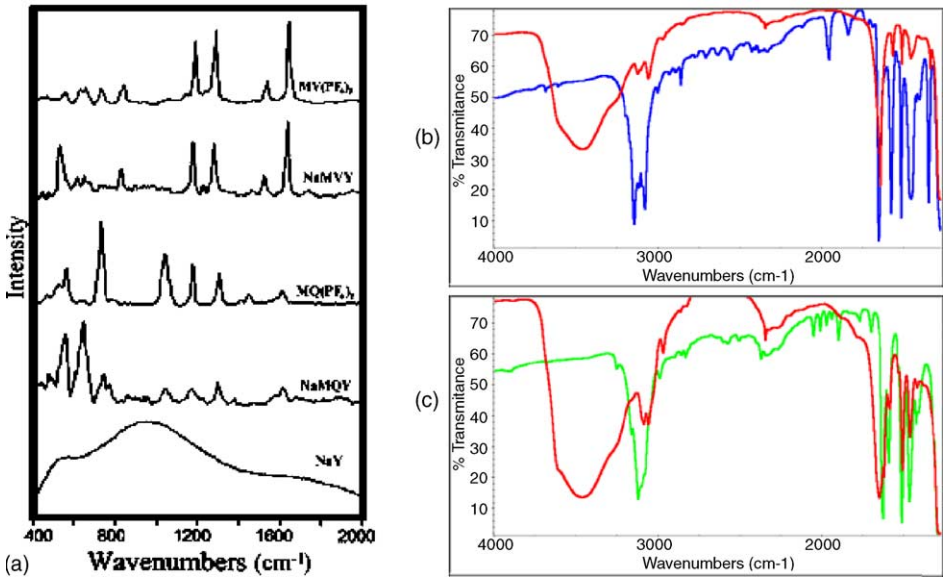


Fig. 10. (a) Raman spectra of viologen hexafluorophosphate salts and viologen doped NaY. IR spectra (4000–1270 $cm^{-1}$) recorded in: (b) Fluorolube of NaMVY (red) and $MV(PF_6)_2$ (blue); (c) Fluorolube of NaMQY (red) and $MQ(PF_6)_2$ (green).

diminishes the importance of the conproportionation argues that the reduction is occurring outside of the zeolite supercage structure [72]. The electrochemical behavior of a viologen containing PMO of the MCM-41 type has also recently been reported [73]. The as-synthesized structure directing agent (cetyltrimethylammonium) filled material is nearly electrochemically inert but the extracted material void of the structure directing agent exhibits two well resolved reduction peaks at −0.36 and −0.75 V versus AgCl/Ag.

## 4. Reactions of viologen/zeolite host–guest complexes

### 4.1. Reduction

In 1995, Kevan and coworkers [74] reported that irradiation of a series of *n*-alkyl substituted 4,4′-viologens at 77 K in dehydrated zeolites X, Y, and A resulted in formation of a light blue colored zeolite. This characteristic color and a single ESR line with a g value of 2.0033 is consistent with formation of the radical cation. Subsequent work with both conventional and laser light sources have demonstrated that the photoyield of radical cation is a function of the donor strength of the zeolite and is far larger than can be accounted for by the presence of defect sites [44,75]. Furthermore, laser flash photolysis experiments demonstrated that both the formation and disappearance of $MV^{+\bullet}$ in a series of alkali exchanged Y zeolites was critically dependent on the identity of the counterion [44]. In the cases of MV/RbNaY and MV/CsNaY, $MV^{+\bullet}$ is so long lived that it can be monitored conveniently by conventional diffuse reflectance spectroscopy. These observations led to the suggestion that excited viologens abstract an electron from the oxygen bridges in the framework of the zeolite and that back electron transfer to regenerate the ground state viologen limits their lifetimes. Estimations of the oxidation potential of $[MV^{2+}]^*$ both in solution (3.65 V versus NHE) [59] and in the zeolite (3.1 V versus SCE) [44] provide evidence for its potent oxidizing power and evidence that the redox potential of the zeolite framework is less than 3.1 V.

Photoreduction of $MV^{2+}$ also occurs by irradiation at 406.7 nm in silver cluster doped NaY [76]. Direct reduction by the zeolite framework does not occur at this wavelength, however, the silver clusters do absorbed at 406 nm and as a consequence the optically excited surface plasmon of the Ag particles is responsible for the reduction.

The corresponding thermal initiated reductions of viologens have occasionally been suggested [77,78]. However, this process appears to be far less efficient with formation of the radical cation often not visibly apparent [78]. For example, heating of several $MV^{2+}$ alkali metal exchanged Y zeolites at temperatures below 200 °C did not did not lead to any visibly detectable formation of $MV^{+\bullet}$ [44].

A very convenient reduction of intercalated viologens by solvated electrons has been reported by Yoon and coworkers [79]. This procedure involves addition of the dry viologen embedded zeolite to a diethylether solution of slightly more than one equivalent of 18-crown-6 and potassium. The use of excess solvated electrons results in over reduction of the viologen moiety.

Carbonylmanganate anions have also been introduced as convenient reducing agents [80]. The addition of $Na^+Mn(CO)_5^-$ to $MV^{2+}$@NaY in a THF or acetonitrile slurry resulted in rapid formation of a blue zeolite powder and quantitative formation of $Mn_2(CO)_{10}$ exclusively in the supernatant solution. This suggests that the anion does not have to migrate into the zeolite for quantitative reduction to occur. This suggestion was verified by the rapid and quantitative reduction with the sodium salt of $Mn(CO)_4P(OPh)_3^-$, which is too large to enter the zeolite. The lack of size selectivity for the anion requires a mechanism for transport of the electron into the pore system of the zeolite. The authors suggested an electron conduction mechanism in which $MV^{+\bullet}$ acts as an electron relay agent via donation to a $MV^{2+}$ in an adjacent supercage by close approach at the supercage window.

In contrast, the carbonylmanganate reduction appears to be highly sensitive to the size of the cationic counterion. The reduction is quantitative with $Na^+$ but decreases in efficiency with increasing size of the counterion. However, even with size excluded counterion 1% reduction was still observed. This was attributed to reduction of $MV^{2+}$ only in the peripheral supercages where the large cation can remain near the external surface of the zeolite to provide electrical neutrality.

### 4.2. Formation, reactions and characterization of charge transfer complexes

In a seminal contribution [41], Yoon and Kochi in 1989 reported that addition of a series of arenes to $MV^{2+}$ or $DQ^{2+}$ embedded NaY generated highly colored intra-zeolite viologen/arene charge transfer complexes [43,81]. The linear correlation of the diffuse reflectance absorption maximum with the ionization potential (IP) of the arenes is in accord with Mulliken theory and provided compelling evidence for the charge-transfer character of the intra-zeolite species [42]. From a practical viewpoint intra-zeolite formations of the charge transfer complexes provide a visual probe for shape-selective absorption and also a means to characterize the kinetic diameter of the arenes [82]. In addition, careful examination of the charge transfer bands provide a unique opportunity to explore the character of the intrazeolite environment. For example, bathochromic shifts of intrazeolite charge transfer maxima can be used to detect absorption of water [83] and changes in the intensity of the bands have been attributed to changes in the free volume available to the CT complex in the zeolite [84]. Similar studies with neutral 1,2,4,5-tetracyanobenzene/arene CT complexes have also been reported [85,86]. Unlike the viologen CT complexes these neutral CT complexes also exhibit emission providing

an advantage and an additional tool to explore the intrazeolite environment.

Formation of intrazeolite $MV^{2+}$ and $DQ^{2+}$ iodide charge transfer complexes have also been reported by treatment of acetonitrile slurries of the viologen embedded zeolite with sodium iodide [87]. These materials exhibit a remarkable range of colors that depend on the concentration of NaI used during their synthesis. For example, $MV^{2+}$ proceeds from yellow to red and $DQ^{2+}$ from orange to deep purple as the concentration of NaI is increased. The diffuse reflectance spectra of the $MV^{2+}$/NaY/$I^-$ CT complex at low concentrations of iodide is characterized by a well-resolved CT band at $\lambda_{MAX} = 362$ nm, while at intermediate concentrations two resolved bands at $\lambda_{MAX} = 362$ and 528 nm were evident. An examination of the spectral changes as a function of NaI concentration allowed assignment of the band at 362 nm to a contact ion pair, $MV^{2+}[I^-]$, and the band at 528 nm to the ion triplet, $MV^{2+}[I^-]_2$. These bands are not resolved in solution preventing quantitative determination of the equilibrium constants for their formations. The unique ability to observe the separate equilibria in NaY may be a result of pressure effects which force unique intra-charge transfer complex distances, especially in the ion triplet, which generates dramatic spectral shifts. Addition of tetramethyl and tetraethylammonium iodide produced exclusively the ion pairs with no trace of ion triplets. This difference, in comparison to NaI, is indicative of ion pair intercalation and the accompanying shape selectivity. Consistent with this interpretation is the complete lack of iodide charge transfer complex formation when NaMVY is treated with the very large tetra-*n*-hexylammonium iodide.

Charge transfer complex formation with the framework included 4,4′-viologen embedded in the PMO depicted in Fig. 9 does not appear to be as favorable as CT complex formations described above [51]. This may be a function of the curvature of the PMO framework which prevents close approach to the viologen and hinders CT complex formation.

### 4.3. Photoinduced electron transfer reactions in charge transfer complexes

Irradiation of the intrazeolite CT complexes formed between $MV^{2+}$ and various arenes using 10 ns 355 or 532 nm $Nd^{3+}$/YAG pulses resulted in formation of transients identified as $MV^{+\bullet}$ and the arene radical cation [88]. Examination of these systems with transient diffuse-reflectance laser flash photolysis have also identified three different types of ion pairs with characteristically different lifetimes from the picosecond to millisecond regime [89]. These lifetimes are an order of magnitude to several orders of magnitude longer than in solution. In analogy to the contact, solvent separated, and free ion pairs observed in solution the different intrazeolite ion pairs were assigned to species with different separation distances. The long lifetimes were attributed to the ability of the negative zeolite framework to pull the ions apart leading to a variety of "internuclear distance isomers" including cage-separated or compartmentalized ions. Parenthetically, similar enhanced lifetimes are not observed in the ionic liquid, 1-butyl-3-methylimidazolium hexafluorophosphate despite similar diffusional and polarity restrictions in the two media [90]. This suggests that other factors, such as framework enhanced charge separation may be playing a key role in the long lifetimes observed in zeolites [47,91].

### 4.4. Synthesis and reactivity of organized molecular assemblies ($Ru(bpy)_3^{2+}$)

Viologens and zeolites have played an important role in the construction of organized molecular assemblies designed to frustrate back electron transfer (BET) that is responsible for the inefficiency in attempts to store solar energy in photoinduced electron transfer (PET) generated ion pairs [92,93]. These studies provide important information about the features of organized molecular assemblies that control both charge separation and recombination and as a consequence play a pivotal role in the modeling of the electron transport chain in natural photosynthesis.

Zeolites, as a result of their ability to compartmentalize reactants and products, provide an ideal platform for these assemblies since spatial separation of charge is an obvious means to prevent energy wasting back electron transfer. Viologens provide ideal electron transfer partners (but not the only type of component that can be envisioned) in these assemblies since their radical cations are stable, readily detected, and easily incorporated into zeolites. Tris(2,2′-bipyridine)ruthenium(II), $[Ru(bpy)_3^{2+}]$, and its derivatives have often been chosen as the other electron transfer partner in these assemblies because of their well-established photophysics and the ability to place these species either on the surface or in the cages/channels of a variety of zeolites.

Three basically different architectures for these organized molecular assemblies are possible as illustrated in Fig. 11. The donor can reside outside and the acceptor inside (architecture diad-**A**), the donor can reside inside and the acceptor outside (architecture diad-**B**), or the donor and acceptor can both reside within the zeolite pore system (architecture diad-**C**). In addition to these basic diad systems, more complex systems (triads, etc.) that further extend the lifetime of the charge-separated states have also been examined.

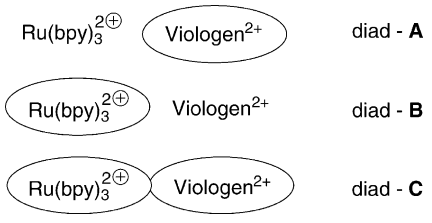


Fig. 11. Molecular assembly architectures.

Dutta and coworkers [94] reported the construction of a diad-**C** (viologen$^{2+}$ = $MV^{2+}$) molecular assembly in zeolite Y in 1987. Laser excitation into the metal to ligand charge transfer (MLCT) band at either 413.1 or 457.9 nm resulted in formation of a blue colored zeolite and the observation of UV-Vis and Raman spectral bands characteristic of the viologen radical cation. The decay of the visible $MV^{+}_{\bullet}$ band at 600 nm over a period of an hour mimicked the recovery of the $Ru(bpy)_3{}^{2+}$ band at 430–460 nm suggesting that the lifetime of the radical cation was limited by back electron transfer. These workers subsequently extended this initial study to a time-resolved-diffuse-reflectance UV-Vis study of diads containing $MV^{2+}$, $DQ^{2+}$, $PQ^{2+}$, and $BQ^{2+}$ [95]. The forward electron transfer rate constants to form $Ru(bpy)_3{}^{3+}$ and the viologen radical cations were greater than $10^7\ s^{-1}$ but the reverse rate constants for $DQ^{2+}$, $PQ^{2+}$, and $BQ^{2+}$ ($4.0 \times 10^4$, $1.1 \times 10^4$, and $7.3 \times 10^3\ s^{-1}$, respectively) decrease with increasing driving force indicating that the back electron transfer is in the Marcus inverted region. Kinetic modeling of the back electron transfer in these systems at high viologen loading levels (1.2–1.7 viologens per supercage) required including a rate constant for electron hopping from viologen-to-viologen. This additional mechanism for charge separation resulted in a larger accumulation of the viologen radical cation than that anticipated by only consideration of the forward and reverse electron transfer rate constants.

Mallouk and coworkers [96] reported the construction of a diad-**A** molecular assembly in zeolite L in 1988. Addition of the tethered donor-acceptor diad **5** to zeolite L resulted in formation of viologen intercalated diad-**A-5**. Irradiation for 10 ns at 532 nm resulted in a transient at 390 nm assigned to the intramolecular charge-separated state $Ru^{3+}$-$DQ^{+}_{\bullet}$ which decayed by a first order process with a lifetime of 0.44 μs. In solution, the lifetime of this state is <5 ns. This work was later extended [65] to a series of 4,4′-bipyridinium ion tethered diads **6** and **7** embedded in zeolite L, Y, and mordenite. The previous suggestion of intercalation of the viologen end into the zeolite was demonstrated with doubly labeled $^{13}CH_3$- NaY diad-**A-6**; only the CP-MAS $^{13}C$ NMR peaks for the accessible methyl groups on the donors were influenced by addition of a paramagnetic probe molecule. The forward first order electron transfer rate constants in diad-**A-6** decrease as a function of increasing

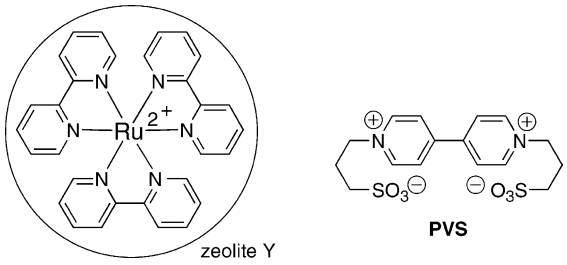


Fig. 12. A diad-**B** molecular assembly.

tether length. In contrast, the quantum yields of charge separation (1–7%) increased and then decreased with tether length with a maximum at $n = 5$. The decreased quantum yields for the longer tether lengths were attributed to competition with other more efficient modes of MLCT (metal-to-ligand-charge-transfer state) decay. The maximum in quantum yield at $n = 5$ was attributed to a combination of slow BET, favorable intermolecular lateral electron transfer on the zeolite surface, and reasonably rapid forward electron transfer quenching of the MLCT state. In addition, diad-**A** systems that have the donor absorbed to the surface rather than tethered to the intrazeolite viologen donor have also been reported [97].

An example of a diad-**B** system is shown in Fig. 12 [98]. Viologen PVS because of its lack of overall charge shows no propensity for migration into the zeolite. Nevertheless, photolysis (420–680 nm) resulted in significant accumulation of the PVS radical anion ($PVS^{-}_{\bullet}$). The charge separation was attributed to, among other factors, electrostatic repulsion between the negatively charged zeolite and the viologen radical anion.

Molecular assemblies with addition complexity (e.g. triads) can be constructed by addition of new components to existing arrays. The new component is thermodynamically chosen (Fig. 13) to function as an electron donor, acceptor, or as an ambiphile (i.e. both electron donor and acceptor). The construction of the new molecular assembly is then done in such a fashion to enhance the lifetime, for example by increasing the spatial separation between the oxidized and reduced centers, of the charge-separated state.

Several successful complex molecular assemblies (CMAs) have been reported [96,98,99]. However, we only illustrate the concept here with the construction of two

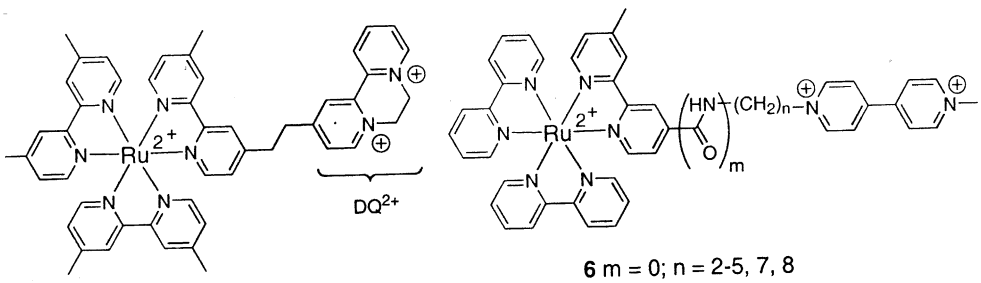

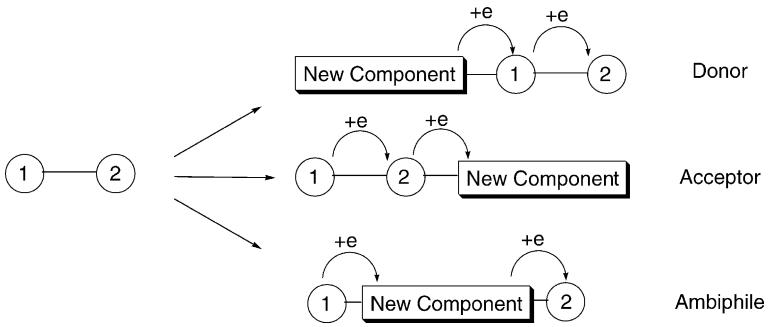


Fig. 13. Construction of complex molecular assemblies (CMA's).

CMAs; a triad and a tetrad (Fig. 14). The triad (A in Fig. 14) [65] consists of a donor, $K_4W(CN)_8{\cdot}2H_2O$, an ambiphile, the $Ru(bpy)_3^{2+}$ derivative, and a tethered mordenite embedded viologen acceptor. This triad results in a five-fold increase, in comparison to the corresponding Ru-tether-viologen diad, in formation of a charge-separated state. The long tether in the diad allows other processes to compete with electron transfer from the MLCT state to form the charge separated configuration. However, in the triad quenching of the photochemically generated MLCT state by $K_4W(CN)_8{\cdot}2H_2O$ competes efficiently with these other processes to generate $Ru(bpy)_3^{+}$ which is a 400 mV better electron donor than the MLCT state, $[Ru(bpy)_3{}^{*2+}]$, and can more easily reduce the viologen. The tetrad (B in Fig. 14) [100] consists of a donor, $Ru(mmb)_3^{2+}$, and two ambiphiles, $Ru(bpy)_2bpz^{2+}$ and $DQ^{2+}$, all embedded in NaY, and an acceptor, PVS, in the surrounding solution. $Ru(mmb)_3^{2+}$ functions in the triad to reduce $Ru(bpy)_2bpz^{3+}$ in order to prevent back electron transfer from $DQ^{+}_{\bullet}$. $DQ^{2+}$ acts as a readily diffusable electron transport agent moving charge from deeply embedded $Ru(bpy)_2bpz^{2+*}$ to PVS in solution.

The viologen/$Ru(bpy)_3^{2+}$ molecular assemblies discussed so far have been investigated in water where ion migration is reasonably facile. Nevertheless, a comparison of the photoinduced growth of $MV^{+}_{\bullet}$ as a function of counterion, M, in $Ru(bpy)_3^{2+}/MV^{2+}/MY$ molecular assemblies show that the

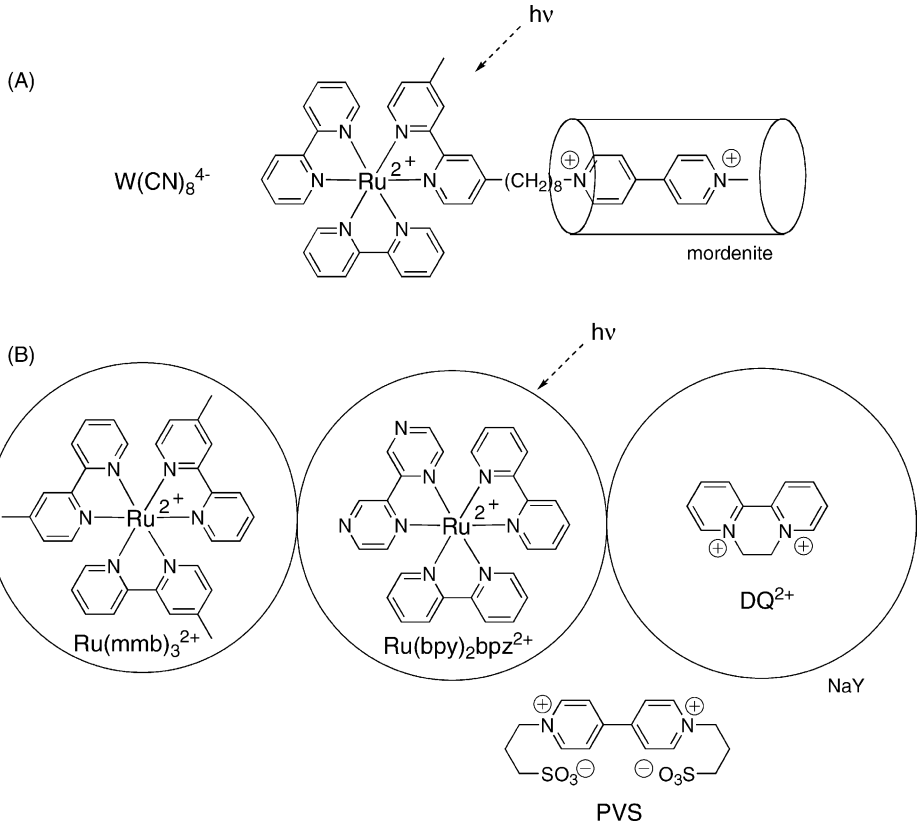


Fig. 14. Examples of two CMA's.

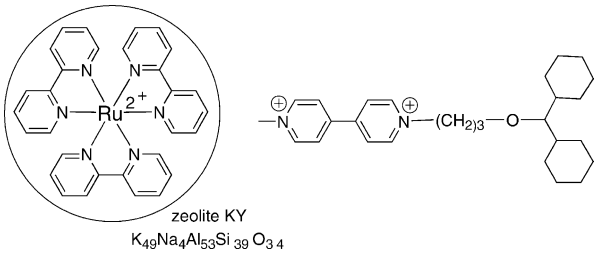


Fig. 15. A diad-**B** molecular assembly.

charge separated states form and decay more rapidly and accumulate to a greater extent in NaY than LiY [101]. This was attributed to the smaller diffusion coefficient for $Li^+$ than $Na^+$ which is a result of its greater affinity for the zeolite framework. The importance of ion migration to insure electrical neutrality was elegantly demonstrated in acetonitrile using the diad-**B** molecular assembly shown in Fig. 15 [78]. The addition of dicyclohexyl-18-crown-6, a potent binder of $K^+$, resulted in over a 10-fold increase in the yield of the charge-separated state. This increase was attributed to the binding of $K^+$ that stabilizes the charge-separated state by 8.9 kcal/mol and mitigates against back electron transfer which must be accompanied by diffusion of $K^+$ back into the zeolite in order to maintain electrical neutrality. A linear increase in the yield of the charge-separated state as a function of the binding constants of a series of crown ethers provided compelling evidence for this suggestion.

Despite the remarkable progress in the construction of molecular assemblies to enhance population of the charge-separated states, challenges still exist to both understand the mechanisms and to harvest the stored energy for useful chemical work. For example, it has now become evident that the yield of the reduced viologen can exceed the amount of available donor, $[Ru(bpy)_3^{2+}]$. In water this has been attributed to a complex process involving formation of a $Ru^{3+}/H_2O$ complex, subsequent oxidation of the viologen to a pyridone, and regeneration of $Ru^{2+}$ [99,102,103]. In acetonitrile this has been attributed to the zeolite host rather than the Ru donor acting as the ultimate electron source [78]. However, the viability of this suggestion has recently been questioned and a concern about the structural integrity of the extensively oxidized zeolite framework has been expressed [104]. In addition, the impact of the recently demonstrated ability of electron transfer from $Ru(bpy)_3^{2+}$ to $MV^{2+}$ to occur through the zeolite framework [91] on the design and mechanistic understanding of molecular assemblies has not yet been fully evaluated.

### 4.5. Miscellaneous reactions

#### 4.5.1. Dehydrogenation reactions

In 2001, Stratakis and Stravroulakis [77] reported that addition of each of the monoterpenes **8a–e** (Fig. 16) to $MV^{2+}$ doped NaY resulted at short reaction times and ambient temperatures in the formation of a mixture of isomeric

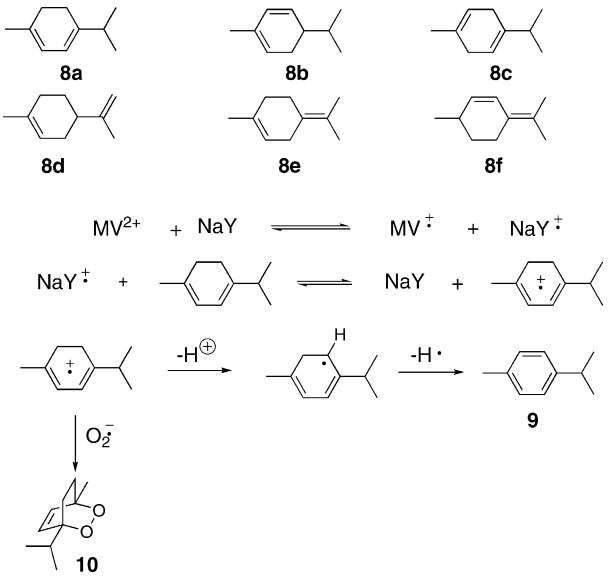


Fig. 16. Mechanism of a zeolite induced dehydrogenation.

monoterpenes which slowly were converted to p-cymene, **9**, as the only product after 45–60 min. In a later manuscript these authors corrected this earlier work reporting that isoterpinolene **8f** rather than terpinolene **8e** was formed as an intermediate terpene that subsequently leads to p-cymene, **9** [105]. Remarkably, the reaction was fairly insensitive to oxygen although formation of a moderate amount (3–15%) of ascaridole, **10**, was reported. The authors suggested that the reaction was initiated by reduction of $MV^{2+}$ by the zeolite (Fig. 16) followed by oxidation of the substrate by the hole created in the zeolite framework. The dehydrogenation reaction appears to be general at least with good hydrogen donors, such as 1,2-dihydronaphthalene and 9,10-dihydroanthracene. Perhaps the most surprising aspect of the reaction is the reduction of the viologen by the zeolite framework. Alvaro et al. [44] reported that heating of a variety of $MV^{2+}$ doped zeolites at temperatures below 200 °C did not lead to any detectable amount of $MV^{+\bullet}$. On the other, hand, Park et al. [78] recently reported that several alkali metal exchanged Y zeolites were capable of thermally reducing the viologen *N*-[3-(dicyclohexylmethyl)oxypropyl]-*N*′-methyl-4,4′-bipyridinium bis-hexafluorophosphate even though its characteristic blue color was not visually apparent. In addition, Alvaro et al. [51] reported a thermal (100 °C) reduction of the framework embedded viologen in the PMO material depicted in Fig. 9. However, in this case even though the source of the reducing electron was not established unequivocally they speculated that residual halide in the PMO might be responsible for the reduction.

#### 4.5.2. Reactions with oxygen

The herbicidal action of viologen radical cations has been attributed in part to their ability to reduce oxygen to form superoxide [2]. Examination of this reaction with $MV^{+\bullet}$ and $DQ^{+\bullet}$ in NaY has provided the first direct evidence for

superoxide formation [29]. These reactions were conducted by adding the radical cation salts, $MV^{+\bullet}PF_6^-$ and $DQ^{+\bullet}PF_6^-$ to NaY then introducing oxygen while monitoring the ESR spectrum of the blue ($MV^{+\bullet}PF_6^-$) and green ($DQ^{+\bullet}PF_6^-$) zeolite powders. The blue color of NaY@$MV^{+\bullet}PF_6^-$ immediately disappeared at −78 °C concomitant with formation of the ESR spectra of superoxide. On the other hand, the bleaching of the green color of NaY@$DQ^{+\bullet}PF_6^-$ required 10 min reflecting the smaller driving force for the $DQ^{+\bullet}$ than the $MV^{+\bullet}$ reduction of oxygen (Table 1). In addition, the difference in $\Delta E^0$ of 0.06 V is sufficient to made the reduction of oxygen with NaY@$DQ^{+\bullet}PF_6^-$ reversible but irreversible with NaY@$MV^{+\bullet}PF_6^-$.

### 4.5.3. Hydrogen evolution

In 1987 Mallouk and coworkers [106] reported a novel $MV^{2+}$ zeolite-L based array for the generation of hydrogen. Zeolite-L is a channel zeolite with the structure depicted in Fig. 17. It consists of a series of six cancrinite cages (Fig. 17a) connected via the four rings to form a 12-ring channel as shown in Fig. 17b. The circle in Fig. 17b circumscribes a cancrinite unit looking down the axis indicated by the arrow in Fig. 17a. The channel structure shown in Fig. 17c is comprised of a series of 0.75 nm sections that share the 12-rings. The 12-rings provide a 0.71 nm entry into the channel system. The largest free diameter is approximately 1.3 nm and lies equidistant from the adjacent 12-rings.

The $MV^{2+}$/zeolite-L based array used to generate hydrogen is shown in Fig. 18. Hydrogen evolution was observed

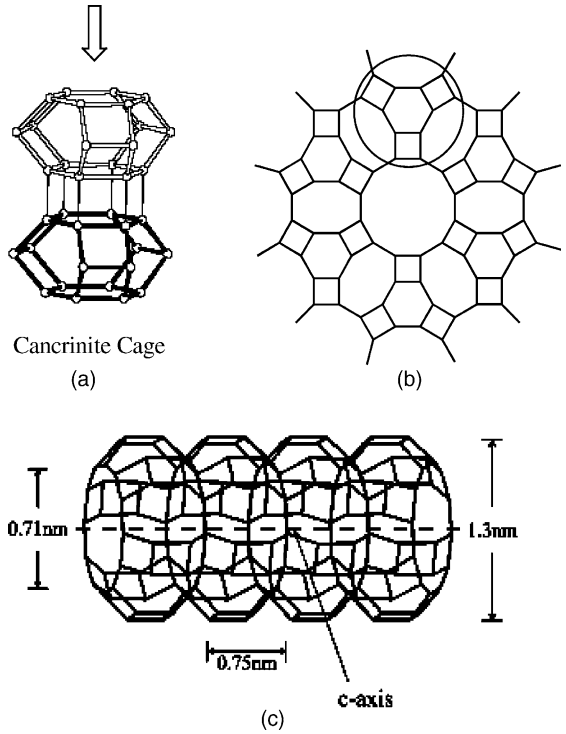


Fig. 17. Structure of zeolite-L.

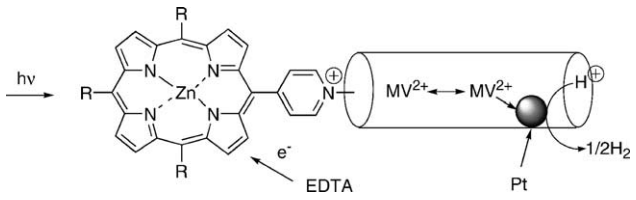


Fig. 18. Hydrogen generation array.

at pH 4.0 in aqueous EDTA which served as a sacrificial electron donor. Substantial hydrogen evolution was observed only at high $MV^{2+}$ loadings suggesting that close $MV^{2+}$–$MV^{2+}$ and porphyrin–$MV^{2+}$ contacts are required. The quantum yield for this first generation heterogeneous composite (lower limit 0.003%) is likely to be improved by use of more complex interfacial assemblies.

## References

[1] L.A. Summers, in: A.R. Katritzky (Ed.), Advances in Heterocyclic Chemistry, vol. 35, Academic Press, Orlando, FL, 1984, pp. 281–374.
[2] L.A. Summers, The Bipyridinium Herbicides, Academic Press, New York, NY, 1980.
[3] P.M.S. Monk, The Viologens, Physicochemical Properties, Synthesis and Applications of the Salts of 4,4′-Bipyridine, Wiley, Chichester, UK, 1998.
[4] J.A. Rabo (Ed.), As a starting point to the extensive zeolite literature, Zeolite Chemistry and Catalysis, vol. 171, American Chemical Society, Washington, DC, 1976.
[5] S. Bhatia, Zeolite Catalysis: Principles and Applications, CRC Press, Boca Raton, Florida, 1990.
[6] H. García, H.D. Roth, Chem. Rev. 102 (2002) 3947.
[7] H.A. Gemborys, B.R.J. Shaw, Electroanal. Interf. Electrochem. 208 (1986) 95.
[8] E.L. Clennan, in: V. Ramamurthy, K.S. Schanze (Eds.), Photochemistry of Organic Molecules in Isotropic and Anisotropic Media, vol. 9, Marcel Dekker, New York, 2003, pp. 275–308.
[9] C.S. Cundy, P.A. Cox, Chem. Rev. 103 (2003) 663.
[10] N.Y. Chen, W.E. Garwood, F.G. Dwyer, Shape Selective Catalysis in Industrial Applications, second ed., Marcel Dekker, New York, 1996.
[11] (a) From IZA website http://www.iza-online.org/.;
(b) E.L. Clennan, A. Pace, F. Jensen, unpublished results.
[12] J.S. Beck, J.C. Vartuli, W.J. Roth, M.E. Leonowicz, C.T. Kresge, K.D. Schmitt, C.T.-W. Chu, D.H. Olson, E.W. Sheppard, S.B. McCullen, J.B. Higgins, J.L. Schlenker, J. Am. Chem. Soc. 114 (1992) 10834.
[13] W.F. Hölderich, in: G. Alberti, T. Bein (Eds.), Comprehensive Supramolecular Chemistry, vol. 7, Elsevier, Oxford, UK, 1996, pp. 671–692.
[14] H. Weidel, M. Russo, Monatshefte 3 (1882) 850.
[15] W. Sliwa, Heterocycles 32 (1991) 2241.
[16] C.L. Bird, A.T. Kuhn, Chem. Rev. 10 (1981) 49.
[17] S. Hünig, J. Groß, E.F. Lier, H. Quast, Liebigs Ann. Chem. (1973) 339.
[18] P.D. Sullivan, D.J. Williams, J. Am. Chem. Soc. 98 (1976) 1711.
[19] I. Willner, A. Ayalon, M. Rabinovitz, New J. Chem. 14 (1990) 685.
[20] J.H. Russell, S.C. Wallwork, Acta Cryst. B28 (1972) 1527.
[21] C.K. Prout, P. Murray-Rust, J. Chem. Soc. A (1969) 1520.
[22] T.M. Bockman, J.K. Kochi, J. Org. Chem. 55 (1990) 4127.
[23] E.M. Kosower, J.L. Cotter, J. Am. Chem. Soc. 86 (1964) 5524.

[24] O. Poizat, C. Sourisseau, Y. Mathey, J. Chem. Soc. Faraday Trans. 1 (80) (1984) 3257.
[25] O. Poizat, C. Sourisseau, J. Corset, J. Mol. Struct. 143 (1986) 203.
[26] R.E. Hester, S. Suzuki, J. Phys. Chem. 86 (1982) 4626.
[27] H.-J. Hofmann, R. Cimiraglia, J. Tomasi, J. Mol. Struct. (Theochem.) 139 (1986) 213.
[28] H.-J. Hofmann, R. Cimiraglia, J. Tomasi, J. Chem. Res. -*S.* (1987) 48.
[29] K.B. Yoon, J. Kochi, J. Am. Chem. Soc. 110 (1988) 6586.
[30] A.J. Bard, A. Ledwith, H.J. Shine, in: V. Gold, D. Bethell (Eds.), Advances in Physical Organic Chemistry, vol. 13, Academic Press, London, 1976, pp 155–278.
[31] A. Pace, E.L. Clennan, F. Jensen, J. Singleton, J. Phys. Chem. B (2004) in press.
[32] M. Mohammad, J. Org. Chem. 52 (1987) 2779.
[33] R. Foster, Organic Charge-Transfer Complexes, vol. 15, Academic Press, New York, 1969.
[34] L. Eberson, Electron Transfer Reactions in Organic Chemistry, vol. 25, Springer, Heidelberg, 1987.
[35] S.G. Bertolotti, J.J. Cosa, H.E. Gsponer, C.M. Previtali, Can. J. Chem. 65 (1983) 2425.
[36] P.M.S. Monk, N.M. Hodgkinson, Electrochim. Acta 43 (1998) 245.
[37] W.C. Hammach, H.G. Drickamer, D.N. Hendrickson, Chem. Phys. Lett. 151 (1988) 469.
[38] T.M. Bockman, S.M. Hubig, J.K. Kochi, J. Org. Chem. 62 (1997) 2210.
[39] H. Byrd, E.P. Suponeva, A.B. Bocarsly, M.E. Thompson, Nature 380 (1996) 610.
[40] S.M. Hubig, J.K. Kochi, J. Phys. Chem. 99 (1995) 17585.
[41] K.B. Yoon, J.K. Kochi, J. Am. Chem. Soc. 111 (1989) 1128.
[42] K.B. Yoon, J.K. Kochi, J. Phys. Chem. 95 (1991) 3780.
[43] K.B. Yoon, in: V. Ramamurthy, K.S. Schanze (Eds.), Solid State and Surface Photochemistry, vol. 5, Marcel Dekker, New York, 2000, pp. 143–251.
[44] M. Alvaro, H. García, S. García, F. Márquez, J.C. Scaiano, J. Phys. Chem. B 101 (1997) 3043.
[45] V. Ramamurthy, D.F. Eaton, J.V. Caspar, Acc. Chem. Res. 25 (1992) 299.
[46] PC Model Volume 7.0, Serena Software, Bloomington, IN. On the other hand, the dimensions of $MV^{2+}$ have been cited as 13.4 Å × 6.4 Å × 3.4 Å (length × width × thickness) see P.K. Dutta, W.J. Turbevill, Phys. Chem. 96 (1992) 9410.
[47] M. Alvaro, B. Ferrer, V. Fornés, H. García, J.C. Scaiano, J. Phys. Chem. B 106 (2002) 6815.
[48] See the following reference for a rare example of a ship-in-a-bottle synthesis of a molecule that spans more than a single supercage. M. Alvaro, E. Carbonell, A. Domenech, V. Fornes, H. Garcia, M. Narayana, Chem. Phys. Chem. 4 (2003) 483.
[49] T. Asefa, M.J. MacLachlan, N. Coombs, G.A. Ozin, Nature 402 (1999) 867.
[50] M. Alvaro, B. Ferrer, V. Fornés, H. García, Chem. Commun. (2001) 2546.
[51] M. Alvaro, B. Ferrer, V. Fornes, H. Garcia, Chem. Phys. Chem. 4 (2003) 612.
[52] M. Alvaro, B. Ferrer, H. Garcia, F. Rey, Chem. Commun. (2002) 2012.
[53] G. Kortüm, Reflectance Spectroscopy, Principles, Methods, Applications, Springer, New York, NY, 1969.
[54] J.P. Kuczynski, B.H. Milosavljevic, A.G. Lappin, J.K. Thomas, Chem. Phys. Lett. 104 (1984) 149.
[55] A.W.-H. Mau, J.M. Overbeek, J.W. Loder, W.H.F. Sasse, J. Chem. Soc. Faraday Trans. 2 (82) (1986) 869.
[56] Y.S. Park, S.Y. Um, K.B. Yoon, J. Am. Chem. Soc. 121 (1999) 3193.
[57] M. Alvaro, G.A. Facey, H. García, S. García, J.C. Scaiano, J. Phys. Chem. 100 (1996) 18173.
[58] G. Villemure, C. Detellier, A.G. Szabo, J. Am. Chem. Soc. 108 (1986) 4658.
[59] J. Peon, X. Tan, J.D. Hoerner, C. Xia, Y.F. Luk, B. Kohler, J. Phys. Chem. A 105 (2001) 5768.
[60] A.S. Hopkins, A. Ledwith, M.F. Stam, Chem. Commun. (1970) 494.
[61] G. Villemure, C. Detellier, A.G. Szabo, Langmuir 7 (1991) 1215.
[62] J.R. Schoonover, P. Chen, W.D. Bates, R.B. Dyer, T.J. Meyer, Inorg. Chem. 33 (1994) 793.
[63] Y. Mao, N.E. Breen, J.K. Thomas, J. Phys. Chem. 99 (1995) 9909.
[64] B. Hennessy, S. Megelski, C. Marcolli, V. Shklover, C. Bärlocher, G. Calzaferri, J. Phys. Chem. B 103 (1999) 3340.
[65] E.H. Yonemoto, Y.I. Kim, R.H. Schmehl, J.O. Wallin, B.A. Shoulders, B.R. Richardson, J.F. Haw, T.E. Mallouk, J. Am. Chem. Soc. 116 (1994) 10557.
[66] D.R. Rolison, in: J.C. Jansen, M. Stöcker, H.G. Karger, J. Weitkamp (Eds.), Advanced Zeolite Science and Applications, vol. 85, 1994, Elsevier, Amsterdam, The Netherlands, pp. 543–586.
[67] A. Walcaruis, L. Lamberts, E.G. Derouane, Electrochim. Acta 38 (1993) 2267.
[68] A. Walcaruis, L. Lamberts, E.G. Derouane, Electrochim. Acta 38 (1993) 2257.
[69] T.-W. Hui, M.D. Baker, J. Phys. Chem. B 105 (2001) 3204.
[70] G. Calzaferri, S. Huber, H. Maas, C. Minkowski, Angew. Chem. Int. Ed. 42 (2003) 3732.
[71] G. Calzaferri, M. Lanz, J.-W. Li, Chem. Commun. (1995) 1313.
[72] T.-W. Hui, M.D. Baker, J. Phys. Chem. B 106 (2002) 827.
[73] A. Doménech, M. Alvaro, B. Ferrer, H. García, J. Phys. Chem. B 107 (2003) 12781.
[74] H.J.D. McManus, C. Finel, L. Kevan, Radiat. Phys. Chem. 45 (1995) 761.
[75] K.T. Ranjit, L. Kevan, in: B.R. Aiello, G. Giordano, F. Testa, (Eds.), Impact of Zeolites and other Porous Materials on the New Technologies at the Beginning of the New Millennium, Pts A and B, vol. 142, Elsevier, Amsterdam, 2002, pp. 763–770.
[76] W.S. Szulbinski, Inorg. Chim. Acta 269 (1998) 253.
[77] M. Stratakis, M. Stavroulakis, Tetrahedron Lett. 42 (2001) 6409.
[78] S.Y. Park, E.J. Lee, Y.S. Chun, Y.D. Yoon, K.B. Yoon, J. Am. Chem. Soc. 124 (2002) 7123.
[79] Y.S. Park, K. Lee, C. Lee, K.B. Yoon, Langmuir 16 (2000) 4470.
[80] K.B. Yoon, Y.S. Park, J.K. Kochi, J. Am. Chem. Soc. 118 (1996) 12710.
[81] K.B. Yoon, Chem. Rev. 93 (1993) 321.
[82] K.B. Yoon, T.J. Huh, J. Phys. Chem. 97 (1993) 6492.
[83] K.B. Yoon, T.J. Huh, J. Phys. Chem. 99 (1995) 7042.
[84] M. Alvaro, H. García, S. García, L. Fernández, Tetrahedron Lett. 37 (1996) 2873.
[85] S. Hashimoto, N. Hagiwara, T. Asahi, H. Masuhara, Langmuir 15 (1999) 3123.
[86] S. Hashimoto, Tetrahedron 56 (2000) 6957.
[87] K.B. Yoon, J.K. Kochi, J. Phys. Chem. 95 (1991) 1348.
[88] S. Sankararaman, K.B. Yoon, T. Yabe, J.K. Kochi, J. Am. Chem. Soc. 113 (1991) 1419.
[89] K.B. Yoon, S.M. Hubig, J.K. Kochi, J. Phys. Chem. 98 (1994) 3865.
[90] M. Álvaro, B. Ferrer, H. Garciá, M. Narayana, Chem. Phys. Lett. 362 (2002) 435.
[91] A. Corma, V. Fornés, M.S. Galletero, H. García, J.C. Scaiano, Chem. Commun. (2002) 334.
[92] J.R. Kincaid, Chem. Eur. J. 6 (2000) 4055.
[93] A.S. Vaidyalingam, M.A. Coutant, P.K. Dutta, in: V. Balzani (Ed.), Electron Transfer in Chemistry, vol. 4, Wiley, Weinheim, Germany, 2001, pp. 412–486.
[94] P.K. Dutta, J.A. Incavo, J. Phys. Chem. 91 (1987) 4443.
[95] M. Vitale, N.B. Castagnola, N.J. Ortins, J.A. Brooke, A. Vaidyalingam, P.K. Dutta, J. Phys. Chem. B 103 (1999) 2408.
[96] J.S. Krueger, J.E. Mayer, T.E. Mallouk, J. Am. Chem. Soc. 110 (1988) 8232.
[97] Y.I. Kim, T.E. Mallouk, J. Phys. Chem. 96 (1992) 2879.
[98] M. Borja, P.K. Dutta, Nature 362 (1993) 43.
[99] Y. Kim, H. Lee, P.K. Dutta, A. Das, Inorg. Chem. 42 (2003) 4215.

[100] M. Sykora, J.R. Kincaid, Nature 387 (1997) 162.
[101] P.K. Dutta, W. Turbeville, J. Phys. Chem. 96 (1992) 9410.
[102] S.K. Das, P.K. Dutta, Langmuir 14 (1998) 5121.
[103] M.A. Coutant, T. Le, N. Castagnola, P.K. Dutta, J. Phys. Chem. B 104 (2000) 10783.
[104] S. Hashimoto, J. Photochem. Photobiol. C 4 (2003) 19.
[105] M. Stratakis, M. Stavroulakis, N. Sofikiti, J. Phys. Org. Chem. 16 (2003) 16.
[106] L. Persaud, A.J. Bard, A. Campion, M.A. Fox, T.E. Mallouk, S.E. Webber, J.M. White, J. Am. Chem. Soc. 109 (1987) 7309.